BB

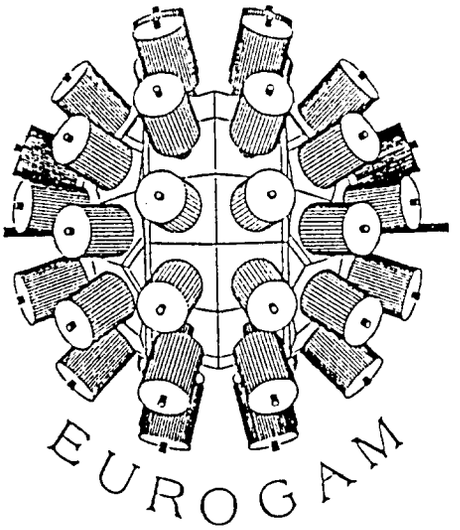

FRANCE - UK

Collaboration

High Spin States in the Nucleus ^{150}Tb

G.Duchêne[1], C.M.Petrache[1], C.W.Beausang[2], F.A.Beck[1], Th.Byrski[1], D.Curien[1], P.J.Dagnall[2], S.Flibotte[1], P.D.Forsyth[2], G.de France[1], B.Haas[1], B.Kharraja[1], J.C.Merdinger[1], D.Prévost[1], C.Schück[3], C.Theisen[1], P.J.Twin[2], J.P.Vivien[1]

[1] *Centre de Recherches Nucléaires, Institut National de Physique Nucléaire et de Physique des Particules, Centre National de la Recherche Scientifique, Université Louis Pasteur, F-67037 Strasbourg Cedex 2, France*

[2] *Oliver Lodge Laboratory, University of Liverpool, Liverpool L69 3BX, United Kingdom*

[3] *Centre de Spectrométrie Nucléaire et de Spectrométrie de Masse, Institut National de Physique Nucléaire et de Physique des Particules, Centre National de la Recherche Scientifique, F-91405 Orsay, France*

Submitted to Zeitschrift für Physik A

CENTRE DE RECHERCHES NUCLEAIRES
STRASBOURG

IN2P3
CNRS

UNIVERSITE
LOUIS PASTEUR

High Spin States in the Nucleus ^{150}Tb

G. Duchêne[1], C. M. Petrache[1,*], C. W. Beausang[2], F. A. Beck[1], Th. Byrski[1], D. Curien[1], P. J. Dagnall[2], S. Flibotte[1], P. D. Forsyth[2], G. de France[1], B. Haas[1], B. Kharraja[1], J. C. Merdinger[1], D. Prévost[1], C. Schück[3], C. Theisen[1], P. J. Twin[2], J. P. Vivien[1]

[1] Centre de Recherches Nucléaires, Institut National de Physique Nucléaire et de Physique des Particules, Centre National de la Recherche Scientifique, Université Louis Pasteur, F-67037 Strasbourg Cedex, France

[2] Oliver Lodge Laboratory, University of Liverpool, Liverpool L69 3BX, United Kingdom

[3] Centre de Spectrométrie Nucléaire et de Spectrométrie de Masse, Institut National de Physique Nucléaire et de Physique des Particules, Centre National de la Recherche Scientifique, F-91405 Orsay, France

Abstract

Excited states in the nucleus ^{150}Tb have been investigated up to spin $39\hbar$ and 13 MeV excitation energy using the ^{130}Te(^{27}Al,7n) reaction and the EUROGAM array. The theoretical interpretation of the observed states has been performed in the framework of the Deformed Independent Particle Model. The analysis of the decay out of the yrast superdeformed band indicates that normal-deformed states with spins between $24\hbar$ and $28\hbar$ are fed.

* On leave from Institute of Physics and Nuclear Engineering, P.O.Box MG-6, Bucharest, Romania.

1. Introduction

With the advent of the new generation of gamma-ray spectrometers (EUROGAM [1,2], GASP [3], GAMMASPHERE [4]), which allow the observation of very weakly populated states at low spin, yrare states well above the yrast line and very high spin states, a more detailed analysis of nuclear level schemes is now possible. In recent years many experimental studies of Tb isotopes were devoted to the search for superdeformed bands [5-10] and only scarce and limited informations about the high spin normal-deformed structures in those nuclei were extracted [5,11,12,13]. Such information is essential when investigating the evolution of nuclear shape as a function of spin and excitation energy in nuclei near closed shells, where coexisting spherical-oblate and prolate structures develop at high spin [14], or when trying to trace back the pathways between the superdeformed and normal-deformed minima [15]. The present study of high spin states in ^{150}Tb is part of a systematic investigation of Tb isotopes in order to fix the high spin structures and their associated configurations. Previously, the normal-deformed levels of ^{150}Tb have been studied via the ^{151}Eu(α, 5n) and ^{136}Ce(^{18}O, p3n) reactions [16] up to spin 21$\hbar$, whereas the superdeformed structures have been investigated using the ^{124}Sn(^{31}P, 5n) reaction [9,10].

2. Experimental methods and results

The decay scheme of ^{150}Tb has been studied using the EUROGAM spectrometer built by a joint France-UK collaboration [1,2]. It consists of 45 large volume germanium detectors (42 were operational in this experiment) of $\geq$70 % relative efficiency (compared to a 3" $\times$ 3" NaI at a γ-ray energy of 1.33 MeV) and this leeds to a full energy peak efficiency of $\approx$4.5 % for the whole array. Each detector is surrounded by bismuth germanate scintillators to reduce the Compton background, leading to a peak-to-total ratio of about 0.55 with a ^{60}Co source. The experiment was carried out at the Daresbury Nuclear Structure Facility. The ^{150}Tb nucleus was populated via the heavy-ion fusion-evaporation reaction ^{130}Te(^{27}Al,7n) at a bombarding energy of 154 MeV. The target of 550 μg.cm^{-2} thickness was evaporated onto a 440 μg.cm^{-2} gold film facing the beam so that ^{150}Tb nuclei were recoiling in vacuum. The counting rate in the individual germanium detectors was about 8 kHz. Unsuppressed events with a γ-ray multiplicity of at least 7 were required, leading to a mean multiplicity value of 3.9 after Compton suppression. A data set of 5.5 $\times$ 10^8 suppressed events was recorded during 80 hours of beam time, corresponding after unpacking to 4.6 $\times$ 10^9 and 3.1 $\times$ 10^9 triple and quadruple coincidences respectively.

The combined effects of high efficiency and sensitivity for high fold coincidences allowed the observation of very weak gamma transitions, with intensities of the order 10^{-2}

compared to the most intense transition in the nucleus using 3 fold coincidences. Examples of coincidence spectra obtained by gating on transitions with very different intensities and placed in various parts of the level scheme are presented in figure 1.

In order to assign spins and tentative parities to the levels, the data were sorted to allow a γ-ray angular distribution analysis. The Ge counters were distributed in rings as follows: 9 detectors at 72°, 4 at 86°, 4 at 94°, 10 at 108°, 10 at 133° and 5 at 157° with respect to the beam axis. To avoid contaminants from nearby nuclei or from multiplets in the same nucleus, we constructed sets of six spectra corresponding to the six rings, double-gated with pairs of carefully selected dipole and quadrupole γ-rays from the main yrast cascade of ^{150}Tb.

Taking into account that there is no evidence for isomers with half-lifes longer than $\sim$1 ns up to high spins [5], which could decay via M2 (magnetic quadrupole) or higher order multipolarity transitions, nearly all ΔI=2 transitions were assumed to have E2 character. For must of the $\Delta I = 1$ transitions, only theoretical considerations which favor one or another configuration were used in order to propose parity assignments to the corresponding levels.

The information about γ-ray energies, intensities, angular distribution coefficients and spin-parity assignments is summarized in table 1. The detailed decay scheme is presented in figure 2.

3. The level scheme of ^{150}Tb

The low part of the level scheme of ^{150}Tb is in very good agreement with the results reported in ref. [16]. A new (15^+) level has been added, connected through the 260.2 and 847.1 keV transitions to the 16^- and 13^+ levels respectively. It has also been possible to firmly fix, by means of the 639.4 keV transition, the position of the 20^+ level. The higher excited levels were also populated in the measurement reported in ref. [9] using the reaction ^{124}Sn(^{31}P, 5n), but the level scheme above the 21^+ state could not be worked out. Only indications that the 188.8, 338.4, 527.2 and 496.5 keV transitions lie above the 21^+ level together with their multipolarity character have previously been given. From the present experiment it turns out that the suggested [9] positions of those transitions on top of the 21^+ level must be changed. Indeed, the observation of the 907.5, 1074.4, 1288.2 and 1340.7 keV transitions enabled us to unambiguously establish the new levels above spin 21^+ and to place the previously reported sequence above spin 25^+. Such high energy transitions have also been observed in the neighbouring ^{151}Tb (ref. [13]) and ^{149}Gd (ref. [17]) nuclei and have been associated with the breaking of the Z=64 proton core.

4. Discussion

The level scheme of ^{150}Tb was interpreted by means of a Deformed Independent Particle Model (D.I.P.M.) [18] which is an improved version of the model presented in ref. [19], involving a deformed single-particle field and a monopole pairing interaction treated by particle-number projection. The non-spherical component of the single-particle field is that of a Nilsson Hamiltonian, while the main spherical single-particle energies are extracted from binding energies and spectroscopic data originating from single-particle stripping and pick-up reactions. The total energy is calculated with a particle number projected B.C.S. wave function and renormalized according to the Strutinsky prescription. The configuration assignment for the main experimental levels are given in table 2. For a level with given spin and parity, the calculated configuration with the lowest excitation energy has been usually adopted. Whenever more than one configuration with similar excitation energies are predicted for a given level, the decay modes of this specific level have been analysed and the configuration in agreement with the most intense observed transitions has been adopted.

4.1. The low spin states

The nucleus ^{150}Tb has one proton and three neutrons outside the Z=64, N=82 ^{146}Gd closed-shell spherical nucleus. The lowest available shell-model orbitals are $s_{1/2}$,$d_{5/2}$ and $h_{11/2}$ for protons and $f_{7/2}$,$h_{9/2}$ and $i_{13/2}$ for neutrons. Due to the fact that the reactions used both in the previous [9,16] and present experiments populate states above the 5.8 min 9^+ isomer, only the level scheme above this state will be discussed in the following. The configuration of the 9^+ isomer involves a proton in the $h_{11/2}$ orbital and the three valence neutrons (among which two are coupled to spin zero) in the $f_{7/2}$ orbital, i.e. $\{\nu\left[(f^2_{7/2})_0 f_{7/2}\right]\otimes\pi h_{11/2}\}_{9^+}$. As for other nuclei in this mass region, the lowest excited states are built on single-particle excitations of the unpaired neutron, i.e. the promotion from the $f_{7/2}$ to the $h_{9/2}$ or $i_{13/2}$ orbitals. The corresponding excitations leed to the 10^+ and 12^- states, which are formed by coupling the $h_{11/2}$ proton with the unpaired valence neutron in the $h_{9/2}$ and $i_{13/2}$ orbitals respectively. The positive-parity 11^+ and 13^+ states have been interpreted as members of the $\nu f^3_{7/2}\otimes\pi h_{11/2}$ multiplet, whereas the 14^+ and 16^+ states as possible members of the $\nu(f^2_{7/2})h_{9/2}\otimes\pi h_{11/2}$ multiplet. The state with spin (15^+) has been explained as a proton in the $h_{11/2}$ orbital coupled to the $19/2^-$ state in ^{149}Gd core for which a $\left[\nu f^3_{7/2}\otimes(3^-)^2\right]_{19/2^-}$ configuration has been assigned [20].

The negative-parity states are expected to have a large admixture of octupole vibrations, a feature which is common to the nuclei around the ^{146}Gd core [21]. Indeed, the strongly populated cascade with spins 10^-, 11^-, 13^-, 15^- can be nicely interpreted by

coupling the odd proton in the $h_{11/2}$ orbital to the $\nu f_{7/2}^3 \otimes 3^-$ multiplet in ^{149}Gd (see ref. [20]). The negative-parity states with even spins up to 18^- can be considered as a band built on the configuration with one neutron excited in the $i_{13/2}$ orbital and coupled to the $h_{11/2}$ proton. However, in this band one expects a non negligible admixture between the $\nu i_{13/2}$ and $(\nu f_{7/2} \otimes 3^-)_{13/2}$ configurations, which could account for the connecting transitions to the odd-spin negative-parity states. Concerning the structure of the strongly populated 19^- state one realises that there is no single-particle configuration where the angular momenta of the valence particles are completely aligned to the symmetry axis and which gives the proper I^π value. However, in the neighbouring ^{149}Gd isotone there exists a $27/2^+$ isomer with a half-life of 6 ns and for which the $\nu(f_{7/2}^2 h_{9/2})_{21/2}^{max} \otimes 3^-$ configuration has been proposed [20]. We therefore expect that the main contribution to the 19^- state in ^{150}Tb originates from the coupling of the $h_{11/2}$ proton with the $27/2^+$ state in ^{149}Gd core. Admixtures with the $\left[\nu(f_{7/2}h_{9/2}i_{13/2})_{27/2} \otimes \pi h_{11/2}\right]_{19^-}$ shell-model configuration could very well account for the transition connecting the maximum aligned 20^- state (having a $\left[\nu(f_{7/2}h_{9/2}i_{13/2})_{29/2}^{max} \otimes \pi h_{11/2}\right]_{20^-}$ proposed configuration) to the 19^- state.

4.2. The high spin states

As in the case of the neighbouring nuclei, in order to generate higher angular momenta one must envisage either the excitation of the valence neutrons into the $i_{13/2}$ orbit and the alignment of their spins along the symmetry axis or the breaking of the proton core and the promotion of another proton to the $h_{11/2}$ orbital [12,13]. Hence, for the positive-parity states 19^+, 20^+ and 21^+, configurations with two neutrons excited in the $i_{13/2}$ orbital coupled to a $h_{11/2}$ proton have been assigned. For the other levels up to spin 25^+ the suggested configurations have one proton promoted from the $d_{5/2}$ or $g_{7/2}$ orbitals to the $h_{11/2}$ orbital and the valence neutrons excited into the lowest available states. At higher spins another proton is further promoted across the $d_{5/2} - h_{11/2}$ gap, while above the 30^- state the promotion of a neutron from the very oblate driving $\nu d_{3/2}$ orbital located below the Fermi surface begins to compete with the proton excitations.

In general, we can say that most of the yrast states have been assigned as maximum aligned configurations and that the nuclear shape changes from nearly spherical to oblate with increasing angular momentum and excitation energy (see table 2).

5. The decay-out of the yrast superdeformed band

Special attention has been paid during the analysis to the transitions which appear to be in coincidence with the yrast superdeformed band of the ^{150}Tb nucleus [9,10]. Due to the detailed knowledge of the normal-deformed level scheme established in the present work, we have been able to trace back the highest normal-deformed levels (and consequently the highest spins) fed by the yrast superdeformed band. From the present experiment we confirm that the previously reported 188.8, 338.4, 496.5 and 527.2 keV transitions [9] are in coincidence with the yrast SD band. In addition we have also observed in coincidence with the SD band the 285.3 and 318.4 keV transitions deexciting the 24^+ and 25^+ levels respectively. From the analysis of the transition intensities, it turns out that states between 24^+ and 28^- are populated and the deduced average entry-spin is $\langle I \rangle \approx 26\hbar$. This value is close to the $\langle I \rangle \approx 27.5\ \hbar$ value determined for the yrast SD band in ^{151}Tb (ref. [13]) or to the $\langle I \rangle \approx 24.5\hbar$ value measured for the yrast SD band in ^{149}Gd (ref. [22]), but is definitely higher compared to the value $\langle I \rangle \approx 21\hbar$ deduced both for the yrast SD band in ^{152}Dy (ref. [23]) and the first excited SD band in ^{151}Tb (identical to the ^{152}Dy yrast SD band) (ref. [13]).

It therefore seems that in the A=150 mass region the average entry-spins into the normal-deformed states after the deexcitation of the SD bands depend weakly on their associated high-N neutron intruder configurations($\nu 7^1$ or $\nu 7^2$), except for the yrast SD band in ^{152}Dy and its twin band (first excited SD band) in ^{151}Tb, which have the same high-N $\pi 6^4 \otimes \nu 7^2$ configuration. For the two later bands, the well defined shell-gaps for Z=66, N=86 at large deformation are probably responsible for the smaller average entry-spin values [7]. We believe that the experimental determination of the average entry-spins into normal-deformed states could impose constraints to the models assuming a statistical process for the deexcitation of the SD bands [24,25]. In such models, where the decay-out mechanism is studied as a barrier penetration problem, it is found that the effects of pairing correlations on the potential energy and the mass tensor are essential in order to account for the rapid depopulation of the SD bands. Moreover, the absolute decay-out spin values (related to the average entry-spins) depend critically on the angular momentum dependence of the normal-deformed level density [25]. The presently available data on average entry-spins indicate that in addition to pairing correlations both the detailed normal-deformed level structures and the configurations of the SD bands must be taken into account when calculating the decay-out spin values.

6. Conclusions

In this work we have established the decay scheme of ^{150}Tb up to high spin ($39\hbar$) and

excitation energy (13 MeV). Configurations in terms of nearly spherical or oblate single-particle orbitals are suggested for most of the observed states. The decay-out study of the yrast superdeformed band indicates an average entry-spin in the normal-deformed level scheme of $\langle I \rangle \approx 26\hbar$.

References

1. Beck, F.A.: Prog. Part. Nucl. Phys. **28**, 443 (1992)
2. Beausang, C.W., Forbes, S.A., Fallon, P., Nolan, P.J., Twin, P.J., Mo, J.N., Lisle, J.C., Bentley, M.A., Simpson, J., Beck, F.A., Curien, D., deFrance, G., Duchêne, G., Popescu, D.G.: Nucl. Instr. and Meth. **A313**, 37 (1992)
3. Bazzacco, D.: Proc. Int. Conf. on Nuclear Structure at High Angular Momentum, Ottawa, AECL 10613, Vol.2, p.376 (1992)
4. Lee, I.Y.: Nucl. Phys. **A520**, 641c (1990)
5. Curien,D.: Ph.D.Thesis, U.L.P.Strasbourg (1988)
6. Byrski, T., Beck, F.A., Curien, D., Schück, C., Fallon, P., Alderson, A., Ali, I., Bentley, M.A., Bruce, A.M., Forsyth, P.D., Howe, D., Roberts, J.W., Sharpey-Schafer, J.F., Smith, G., Twin, P.J.: Phys. Rev. Lett. **64**, 1650 (1990)
7. Curien, D., de France, G., Beausang, C.W., Beck, F.A., Byrski, T., Clarke, S., Dagnall, P., Duchêne, G., Flibotte, S., Forbes, S., Forsyth, P.D., Haas, B., Joyce, M.A., Kharraja, B., Nyako, B.M., Schück, C., Simpson, J., Theisen, C., Twin, P.J., Vivien, J.P., Zolnai, L.: Phys. Rev. Lett. **71**, 2559 (1993)
8. Fallon, P., Alderson, A., Bentley, M.A., Forsyth, P.D., Howe, D., Roberts, J.W., Sharpey-Schafer, J.F., Twin, P.J., Beck, F.A., Byrski, T., Curien, D., Schück, C.: Phys. Lett. **B218**, 137 (1989)
9. Deleplanque, M.A., Beausang, C.W., Burde, J., Diamond, R.M., Stephens, F.S., McDonald, R.J., Draper, J.E.: Phys. Rev. **C39**, 1651 (1989)
10. Haas, B., Ward, D., Andrews, H.R., Ball, G..C., Drake, T.E., Flibotte, S., Galindo-Uribarri, A., Janzen, V.P., Johansson, J.K., Kluge, H., Kuehner, J., Omar, A., Pilotte, S., Prévost, A., Rodriguez, J., Radford, D.C., Taras, P., Vivien, J.P., Waddington, J.C., Aberg, S.: Phys. Rev. **C42**, R1817 (1990)
11. Meliani, Z., Dionisio, J.S., Körner, E.G., Popescu, D.G., Schück, C., Vieu, Ch., Duchêne, G., Merdinger, J.C., Bendjaballah, N.: J. Phys. **G20**, L7 (1994)
12. Meliani, Z., Dionisio, J.S., Schück, C., Vieu, Ch., Beck, F.A., Byrski, T., Curien, D., Duchêne, G., Merdinger, J.C., Fallon, P., Roberts, J.W., Sharpey-Schafer, J.F.: to be published in Nucl. Phys. A
13. Petrache, C.M., Duchêne, G., Kharraja, B., Beausang, C.W., Beck, F.A., Byrski, T., Curien, D., Dagnall, P., Flibotte, S., Forsyth, P.D., de France, G., Haas, B., Kiss, A., Merdinger, J.C., Prévost, D., Schück, C., Theisen, C., Twin, P.J., Vivien, J.P.: submitted to Nucl. Phys. A

14. Nyakó, B.M., Simpson, J., Twin, P.J., Howe, D., Forsyth, P.D., Sharpey-Schafer, J.F.: Phys. Rev. Lett. **56**, 2680 (1986)

15. Ataç, A., Piiparinen, M., Herskind, B., Nyberg, J., Sletten, G., de Angelis, G., Forbes, S., Gjørup, N., Hagemann, G., Ingebretsen, F., Jensen, H., Jerrestam, D., Kusakari, H., Lieder, R.M., Marti, G.V., Mullins, S., Santonocito, D., Schnare, H., Sträle, K., Sugawara, M., Tjøm, P.O., Virtanen, A., Wadsworth, R.: Phys. Rev. Lett. **70**, 1069 (1993)

16. Broda, R., Ogawa, M., Kleinheintz, P., Sheline, R.K., Richter, L.: Proc. Symp. on High Spin Phenomena in Nuclei, Argonne, ANL/PHY-79-4, p. 401 (1979)

17. Flibotte, S., Haas, B., Banville, F., Gascon, J., Taras, P., Andrews, H.R., Radford, D.C., Ward, D., Waddington, J.C.: Nucl. Phys. **A530**, 187 (1991)

18. Døssing, T., Neergård, K., Sagawa, H.: Phys. Scr. **24**, 258 (1981)

19. Matsuyanagi, K., Døssing, T., Neergård, K.: Nucl. Phys.**A307**, 253 (1978)

20. Piiparinen, M., Pengo, R., Nagai, Y., Hammaren, E., Kleinheinz, P., Roy, N., Carlen, L., Ryde, H., Lindblad, Th., Johnson, A., Hjorth, S.A., Blomqvist, J.: Z. Physik A - Atomic Nuclei **300**, 133 (1981)

21. Kleinheinz, P.: Physica Scripta **24**, 236 (1981)

22. Flibotte, S., et al.: to be published

23. Twin, P.J., Nyakó, B.M., Nelson, A.H., Simpson, J., Bentley, M.A., Cranmer-Gordon, H.W., Forsyth, P.D., Howe, D., Mokhtar, A.R., Morrison, J.D., Sharpey-Schafer, J.F., Sletten, G.: Phys. Rev. Lett. **57**, 811 (1986)

24. Schimizu, Y.R., Barranco, F., Døssing, T., Vigezzi, E., Broglia, R.A.: Proc. of the Workshop-Symposium on "Future Directions in Nuclear Physics with 4π Gamma Detection Systems of the New Generation", Strasbourg, p. 141 (1991)

25. Shimizu, Y.R., Vigezzi, E., Døssing, T., Broglia, R.A.: Nucl. Phys. **A557**, 67c (1993)

Figure Captions

Figure 1. Double-gated coincidence spectra: the first gate used to select the ^{150}Tb nucleus, was set on one of the 276, 355, 502, 677, 759, 766 and 832 keV transitions, whereas the second gate was set either on the 355.6($18^- - 16^-$) keV transition (upper part) or the 1340.7($22^- - 20^-$) keV transition (lower part). The strongest coincident γ rays of ^{150}Tb are marked by their energies in keV.

Figure 2. Level scheme of ^{150}Tb above the 9^+, $T_{1/2}$=5.8 min isomer obtained in the present work.

Table Captions

Table 1. Gamma-ray energies, relative intensities compared to the sum of 594.0, 758.8 and 832.5 keV transitions, angular distribution coefficients and spin-parity assignments for the transitions in ^{150}Tb.

Table 2. Single-particle configuration assignments for the high-spin states in ^{150}Tb. The spins given in parenthesis are not determined experimentally. In columns 2 and 3 are given the experimental and theoretical excitation energies with respect to the 9^+ isomer, whereas in the fourth column the theoretical quadrupole deformations are given.

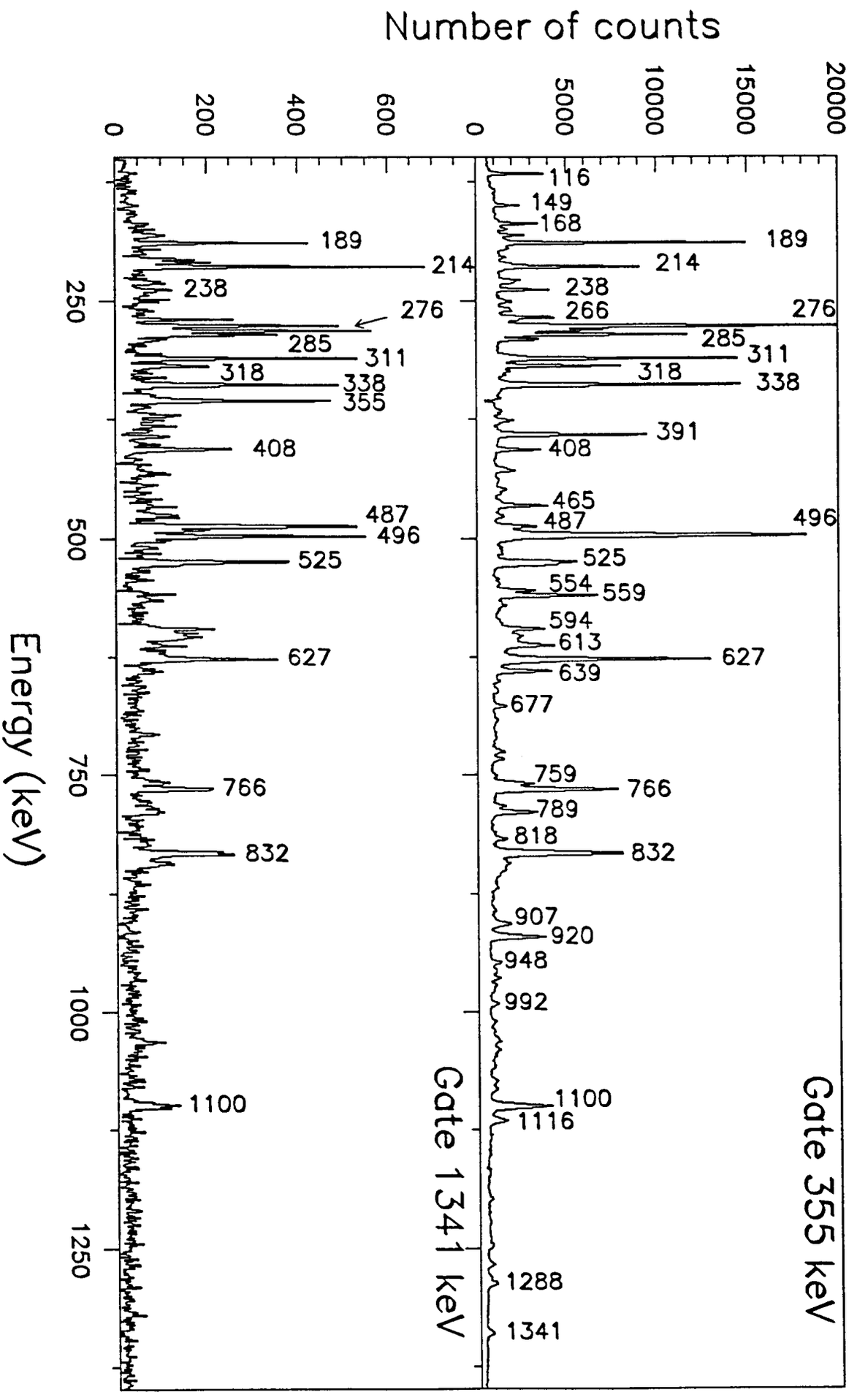
Number of counts
0
200
400
600
0
5000
10000
15000
20000
Energy (keV)
250
500
750
1000
1250
Gate 1341 keV
189
214
238
276
285
311
318
338
355
408
487
496
525
627
766
832
1100
Gate 355 keV
116
149
168
189
214
238
266
276
285
311
318
338
391
408
465
487
496
525
554
559
594
613
627
639
677
759
766
789
818
832
907
920
948
992
1100
1116
1288
1341

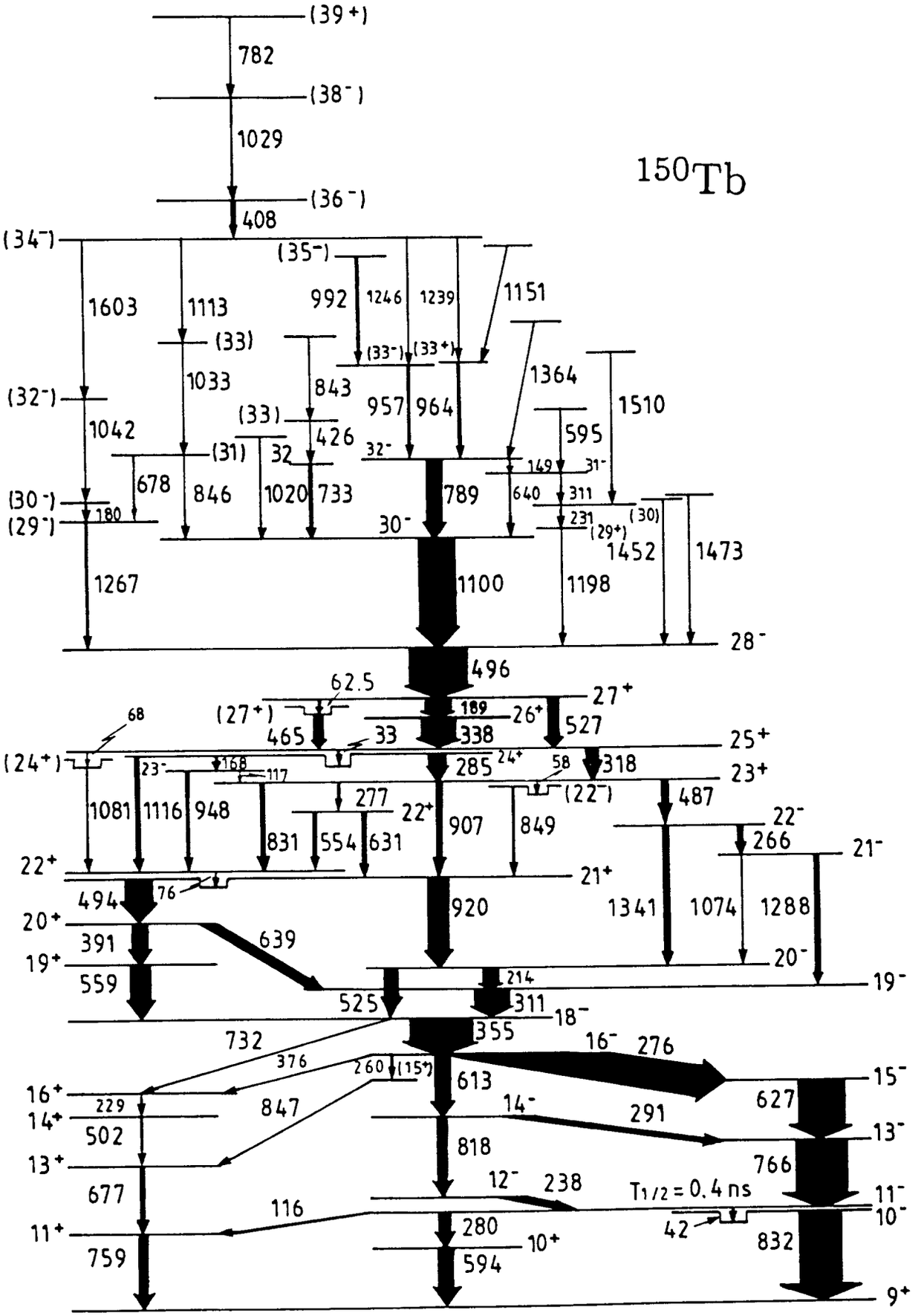
150Tb
(39+)
782
(38-)
1029
(36-)
408
(34-)
(35-)
1603
1113
992
1246
1239
1151
(33)
(33-)
(33+)
1033
843
1364
1510
(32-)
957
964
1042
(33)
426
595
(31)
32
32-
149
31-
678
846
1020
733
789
640
311
(30-)
180
(29-)
30-
231
(29+)
(30)
1452
1473
1267
1100
1198
28-
496
62.5
27+
(27+)
189
26+
527
68
465
33
338
25+
(24+)
23-
168
117
285
24+
58
318
23+
1081
1116
948
277
831
554
631
22+
907
849
(22-)
487
22-
266
21-
22+
21+
494
76
920
1341
1074
1288
20+
391
639
20-
19+
559
214
19-
525
311
18-
732
355
16-
276
376
260
(15+)
613
627
15-
16+
229
847
14-
291
14+
502
818
766
13-
13+
12-
238
T1/2 = 0.4 ns
677
116
11-
10-
11+
280
42
832
759
10+
594
9+

Table 1

Gamma-ray energies, relative intensities compared to the sum of 594.0, 758.8 and 832.5 transitions, angular distribution coefficients[a] and spin-parity assignments for the transitions in ^{150}Tb.

E_γ(keV)	$I_\gamma^{b)}$	a_2	$I_i^\pi \rightarrow I_f^{\pi\,c)}$
115.7	6	0.27 ± 0.12	$11^- \rightarrow 11^+$
116.6	2.2 (0.5)		$23^- \rightarrow 23^+$
149.5	4(1)	-0.14± 0.23	$32^- \rightarrow 31^-$
168.4	4.6	-0.18± 0.24	$24^+ \rightarrow 23^-$
180.1	3.8 (0.5)		$(30^-) \rightarrow (29^-)$
188.8	34	-0.13 ± 0.06	$27^+ \rightarrow 26^+$
213.7	23	-0.14 ± 0.11	$20^- \rightarrow 19^-$
228.7	4(1)		$16^+ \rightarrow 14^+$
230.8	2.2(0.5)		$(30) \rightarrow (29^+)$
238.1	16	-0.14 ± 0.17	$12^- \rightarrow 11^-$
260.2	1.7(0.5)		$16^- \rightarrow (15^+)$
266.2	10	-0.19 ± 0.16	$22^- \rightarrow 21^-$
276.5	71	-0.20 ± 0.05	$16^- \rightarrow 15^-$
277.1	11(2)		$23^+ \rightarrow 22^+$
280.5	21	-0.17 ± 0.13	$11^- \rightarrow 10^+$
285.3	27	-0.13 ± 0.13	$24^+ \rightarrow 23^+$
290.9	9	-0.26± 0.13	$14^- \rightarrow 13^-$
310.9	49	-0.26 ± 0.08	$19^- \rightarrow 18^-$
311.4	< 1		$31^- \rightarrow (30)$
318.4	21	0.19 ± 0.17	$25^+ \rightarrow 23^+$
338.4	51	-0.11 ± 0.07	$26^+ \rightarrow 25^+$
355.6	95	0.27 ± 0.05	$18^- \rightarrow 16^-$
376.0	2.4 (0.5)		$16^- \rightarrow 16^+$
390.7	26	-0.21 ± 0.07	$20^+ \rightarrow 19^+$
407.7	10	0.28 ± 0.21	$(36^-) \rightarrow (34^-)$
426.0	2.9(0.5)		$(33) \rightarrow 32$
465.1	14	0.15 ± 0.36	$27^+ \rightarrow 25^+$
486.9	12	-0.12 ± 0.18	$23^+ \rightarrow 22^-$
494.1	40	-0.35 ±0.15	$21^+ \rightarrow 20^+$
496.5	81	-0.15 ± 0.13	$28^- \rightarrow 27^+$
502.6	5(1)		$14^+ \rightarrow 13^+$
524.6	24	0.34 ± 0.17	$20^- \rightarrow 18^-$
527.2	19	0.35 ± 0.22	$27^+ \rightarrow 25^+$
554.1	9(1)		$22^+ \rightarrow 22^+$
559.6	32	-0.20 ± 0.17	$19^+ \rightarrow 18^-$
594.0	21	-0.29 ± 0.27	$10^+ \rightarrow 9^+$
595.3	< 1		$\rightarrow 31^-$
613.0	26	0.14 ± 0.14	$16^- \rightarrow 14^-$
627.4	71	0.31 ± 0.02	$15^- \rightarrow 13^-$
630.7	10	-0.31 ± 0.21	$22^+ \rightarrow 21^+$
639.4	16		$20^+ \rightarrow 19^-$
640.0	3(1)		$31^- \rightarrow 30^-$
677.5	9(1)		$13^+ \rightarrow 11^+$
678.1	2(1)		$(31) \rightarrow (29^-)$

E_γ(keV)	$I_\gamma^{b)}$	a_2	$I_i^\pi \rightarrow I_f^{\pi\,c)}$
732.1	1.3(0.5)		$18^- \rightarrow 16^+$
733	7(1)	0.27 ± 0.46	$32 \rightarrow 30^-$
758.8	17	0.26 ± 0.20	$11^+ \rightarrow 9^+$
765.7	80	0.32 ± 0.01	$13^- \rightarrow 11^-$
782	4(1)		$(39^+) \rightarrow (38^-)$
789.5	27	0.39 ± 0.21	$32^+ \rightarrow 30^+$
818.5	16	0.34 ± 0.07	$14^- \rightarrow 12^-$
831.2	13(3)		$23^+ \rightarrow 22^+$
832.5	62	0.02 ±0.01	$10^- \rightarrow 9^+$
843	3(1)		$\rightarrow (33)$
846	2(1)		$(31) \rightarrow 30^-$
847.1	3(1)		$(15^+) \rightarrow 13^+$
849.3	3.4(0.5)		$(22^-) \rightarrow 21^+$
907.5	14	0.48 ± 0.21	$23^+ \rightarrow 21^+$
920.1	34	-0.11 ± 0.14	$21^+ \rightarrow 20^-$
947.9	7		$23^- \rightarrow 22^+$
956.7	8(1)		$(33^-) \rightarrow 32^-$
963.8	7(1)		$(33^+) \rightarrow 32^-$
991.9	5		$(35^-) \rightarrow (33^-)$
1020	3.5(0.5)		$\rightarrow 30^-$
1028.8	4(1)	0.12 ± 0.22	$(38^-) \rightarrow (36^-)$
1032.8	4(2)	0.39 ± 0.19	$(33) \rightarrow (31)$
1041.9	3(0.5)	0.42 ± 0.30	$(32^-) \rightarrow (30^-)$
1074.5	3(1)		$21^- \rightarrow 20^-$
1081.0	3.9(0.5)		$(24^+) \rightarrow 22^+$
1100.5	57	0.39 ± 0.19	$30^- \rightarrow 28^-$
1113.1	4(2)		$(34^-) \rightarrow (33)$
1116.1	12	0.30 ± 0.07	$24^+ \rightarrow 22^+$
1151	< 1		$\rightarrow (33^+)$
1198.3	3.7(0.5)		$(29^+) \rightarrow 28^-$
1238.7	< 1		$(34^-) \rightarrow (33^+)$
1245.8	< 2		$(34^-) \rightarrow (33^-)$
1266.9	6.2(0.5)		$(29^-) \rightarrow 28^-$
1288.2	10	0.43 ± 0.53	$21^- \rightarrow 19^-$
1340.7	10(2)	0.16 ± 0.17	$22^- \rightarrow 20^-$
1364	< 1		$\rightarrow 32^-$
1452	1.9 (0.5)		$\rightarrow 28^-$
1472.6	1.4 (0.5)		$\rightarrow 28^-$
1510	< 1		$\rightarrow (30)$
1603.6	1.8 (0.5)		$(34^-) \rightarrow (32^-)$

[a)] The a_4 coefficients are all very close to zero and therefore have not been included in the table.
[b)] Intensities corrected for efficiency and internal conversion, relative to the sum of the intensities of the 594.0, 758.8 and 832.5 keV transitions. Except where stated, the errors are less than 10%.
[c)] The tentative parity of the states are indicated. The spin values for which angular distribution coefficients could not be extracted and which are not fixed by other interband transitions are given in parenthesis.

Table 2

Single-particle configuration assignments for the high-spin states in ^{150}Tb. The spins given in parenthesis are not determined experimentally. In columns 2 and 3 are given the experimental and theoretical excitation energies with respect to the 9^+ isomer, whereas in the fourth column the theoretical quadrupole deformations are given.

I^π	E_{exp} (MeV)	E_{th} (MeV)	β_2	Neutron	Proton
9^+	0.0	0.0	-0.04	$(f^2_{7/2})_0 f_{7/2}$	$h_{11/2}$
10^+	0.594	0.82	-0.07	$(f^2_{7/2})_0 h_{9/2}$	$h_{11/2}$
10^-	0.832	1.66	-0.06	$f^3_{7/2} \otimes 3^-$	$h_{11/2}$
11^+	0.759	1.37	-0.03	$f^3_{7/2}$	$h_{11/2}$
11^-	0.874	1.41	-0.08	$f^3_{7/2} \otimes 3^-$	$h_{11/2}$
12^-	1.113	1.15	-0.08	$(f^2_{7/2})_0 i_{13/2}$	$h_{11/2}$
13^+	1.436	1.28	-0.04	$(f^3_{7/2})^{max}_{15/2}$	$h_{11/2}$
13^-	1.640	2.33	-0.07	$f^3_{7/2} \otimes 3^-$	$h_{11/2}$
14^-	1.931	2.60	-0.07	$f^2_{7/2} i_{13/2}$	$h_{11/2}$
14^+	1.939	2.34	-0.05	$f^2_{7/2} h_{9/2}$	$h_{11/2}$
15^-	2.267	2.76	-0.06	$f^3_{7/2} \otimes 3^-$	$h_{11/2}$
(15^+)	2.284	2.19	-0.06	$f^3_{7/2} \otimes (3^-)^2$	$h_{11/2}$
16^-	2.544	2.76	-0.06	$f^2_{7/2} i_{13/2}$	$h_{11/2}$
16^+	2.168	1.95	-0.06	$(f^2_{7/2} h_{9/2})^{max}_{21/2}$	$h_{11/2}$
18^-	2.900	2.33	-0.07	$(f^2_{7/2} i_{13/2})^{max}_{25/2}$	$h_{11/2}$
19^-	3.211	3.15	-0.09	$(f^2_{7/2} h_{9/2} \otimes 3^-)^{max}_{27/2}$	$h_{11/2}$
19^+	3.459	4.40	-0.06	$f_{7/2} i^2_{13/2}$	$h_{11/2}$
20^-	3.425	2.89	-0.09	$(f_{7/2} h_{9/2} i_{13/2})^{max}_{29/2}$	$h_{11/2}$
20^+	3.850	4.07	-0.09	$f_{7/2} i^2_{13/2}$	$h_{11/2}$
21^+	4.345	3.80	-0.08	$(f_{7/2} i^2_{13/2})^{max}_{31/2}$	$h_{11/2}$
21^-	4.500	4.47	-0.08	$f^2_{7/2} h_{9/2}$	$d^{-1}_{5/2} h^2_{11/2}$
22^+	4.421	4.81	-0.08	$f^2_{7/2} i_{13/2}$	$d^{-1}_{5/2} h^2_{11/2}$
22^-	4.765	4.66	-0.08	$f^2_{7/2} h_{9/2}$	$d^{-1}_{5/2} h^2_{11/2}$
22^+	4.976	5.11	-0.09	$(h_{9/2} i^2_{13/2})^{max}_{33/2}$	$h_{11/2}$
(22^-)	5.194	5.09	-0.08	$f^2_{7/2} h_{9/2}$	$g^{-1}_{7/2} h^2_{11/2}$
23^+	5.252	4.81	-0.08	$f^2_{7/2} i_{13/2}$	$d^{-1}_{5/2} h^2_{11/2}$
23^-	5.369	5.13	-0.07	$(f^2_{7/2} h_{9/2})^{max}_{21/2}$	$(d^{-1}_{5/2} h^2_{11/2})^{max}_{25/2}$
24^+	5.538	5.00	-0.08	$f^2_{7/2} i_{13/2}$	$d^{-1}_{5/2} h^2_{11/2}$
(24^+)	5.502	5.26	-0.10	$f_{7/2} h_{9/2} i_{13/2}$	$d^{-1}_{5/2} h^2_{11/2}$
25^+	5.571	5.50	-0.07	$(f^2_{7/2} i_{13/2})^{max}_{25/2}$	$(d^{-1}_{5/2} h^2_{11/2})^{max}_{25/2}$
26^+	5.909	5.47	-0.10	$f_{7/2} h_{9/2} i_{13/2}$	$d^{-1}_{5/2} h^2_{11/2}$
27^+	6.036	6.47	-0.08	$f_{7/2} h_{9/2} i_{13/2}$	$g^{-1}_{7/2} h^2_{11/2}$
27^+	6.098	6.02	-0.10	$(f_{7/2} h_{9/2} i_{13/2})^{max}_{29/2}$	$(d^{-1}_{5/2} h^2_{11/2})^{max}_{25/2}$
28^-	6.595	6.26	-0.10	$(f_{7/2} h_{9/2} i_{13/2})^{max}_{29/2}$	$(d^{-2}_{5/2})_0 (h^3_{11/2})^{max}_{27/2}$
(29^+)	7.793	7.22	-0.10	$(f_{7/2} i^2_{13/2})^{max}_{31/2}$	$(d^{-2}_{5/2})_0 (h^3_{11/2})^{max}_{27/2}$

I^π	E_{exp} (MeV)	E_{th} (MeV)	β_2	Neutron	Proton
(29^-)	7.862	7.78	-0.11	$f_{7/2}h_{9/2}i_{13/2}$	$d^{-2}_{5/2}h^{3}_{11/2}$
30^-	7.695	8.17	-0.08	$(f^{2}_{7/2}i_{13/2})^{max}_{25/2}$	$(d^{-2}_{5/2}h^{3}_{11/2})^{max}_{35/2}$
(30^-)	8.042	7.78	-0.11	$f_{7/2}h_{9/2}i_{13/2}$	$d^{-2}_{5/2}h^{3}_{11/2}$
31^-	8.335	8.43	-0.10	$f_{7/2}h_{9/2}i_{13/2}$	$d^{-2}_{5/2}h^{3}_{11/2}$
32^-	8.485	8.65	-0.10	$(f_{7/2}h_{9/2}i_{13/2})^{max}_{29/2}$	$(d^{-2}_{5/2}h^{3}_{11/2})^{max}_{35/2}$
(32^-)	9.084	9.10	-0.10	$f_{7/2}h_{9/2}i_{13/2}$	$g^{-1}_{7/2}d^{-1}_{5/2}h^{3}_{11/2}$
(33^-)	9.441	9.53	-0.15	$d^{-1}_{3/2}f_{7/2}h_{9/2}i^{2}_{13/2}$	$(d^{-2}_{5/2})_0h^{3}_{11/2}$
(33^+)	9.449	9.42	-0.15	$d^{-1}_{3/2}f_{7/2}h_{9/2}i^{2}_{13/2}$	$d^{-1}_{5/2}h^{2}_{11/2}$
(34^-)	10.687	9.53	-0.15	$d^{-1}_{3/2}f_{7/2}h_{9/2}i^{2}_{13/2}$	$(d^{-2}_{5/2})_0h^{3}_{11/2}$
(35^-)	10.433	10.60	-0.20	$(d^{-2}_{3/2})_0f^{2}_{7/2}h_{9/2}i^{2}_{13/2}$	$d^{-1}_{5/2}h^{2}_{11/2}$
(36^-)	11.095	10.98	-0.15	$d^{-1}_{3/2}f_{7/2}h_{9/2}i^{2}_{13/2}$	$d^{-2}_{5/2}h^{3}_{11/2}$
(38^-)	12.124	11.94	-0.15	$d^{-1}_{3/2}f_{7/2}h_{9/2}i^{2}_{13/2}$	$d^{-2}_{5/2}h^{3}_{11/2}$
(39^+)	12.906	12.63	-0.20	$(d^{-2}_{3/2})_0f^{2}_{7/2}h_{9/2}i^{2}_{13/2}$	$d^{-2}_{5/2}h^{3}_{11/2}$